Crustal structure of Sri Lanka derived from joint inversion of receiver functions and seismic ambient noise using a Bayesian approach

Jennifer Dreiling[1,2], Frederik Tilmann[1,2], Xiaohui Yuan[1], Christian Haberland[1], S.W. Mahinda Seneviratne[3]

[1]GFZ German Research Centre for Geosciences, Telegrafenberg, 14473 Potsdam, Germany
[2]Freie University of Berlin, Malteserstr. 74−100, 12249 Berlin, Germany
[3]GSMB Geological Survey and Mines Bureau, Sri Lanka

Please note that this is a non-peer-reviewed EarthArXiv preprint, submitted to *J. Geophys. Res. Solide Earth* in September 2019.
`https://eartharxiv.org/`

Key Points:

- Sri Lanka has mostly isostatically compensated 30–40 km thick crust
- Major mid-crustal westward dipping interface related to thrust contact between Highland Complex and Vijayan Complex
- Dipping discontinuity and low velocity zone in Highland Complex support amalgamation theory of stepwise collision

Corresponding author: Jennifer Dreiling, `dreiling@gfz-potsdam.de`

Abstract

We study the crustal structure of Sri Lanka by analyzing data from a temporary seismic network deployed in 2016–2017 to shed light on the amalgamation process from the geophysical perspective. Rayleigh wave phase dispersion from ambient noise cross-correlation and receiver functions were jointly inverted using a transdimensional Bayesian approach.

The Moho depths range between 30 and 40 km, with the thickest crust (38–40 km) beneath the central Highland Complex (HC). The thinnest crust (30–35 km) is found along the west coast, which experienced crustal thinning associated with the formation of the Mannar Basin. The majority of Vp/Vs ratios lies within a range of 1.66–1.8 and predominantly favor a felsic composition with intermediate-to-high silica content of the rocks.

A major intra-crustal (18–27 km), slightly westward dipping ($\sim 4.3°$) interface with high Vs (>4 km/s) underneath is prominent in the central HC, continuing in the eastern Vijayan Complex (VC). The dipping discontinuity and a low velocity zone in the central Highlands can be related to the HC/VC contact zone and is in agreement with a well-established amalgamation hypothesis of a stepwise collision of the arc fragments, including deep crustal thrusting processes and a transpressional regime along the eastern suture between the HC and VC.

1 Introduction

Sri Lanka occupied a key region in both the assembly and the multistage breakup of Gondwana. Many petrological, geochemical and geochronological studies have been conducted to reconstruct the processes acting during the amalgamation. However, little is known about the seismic structure of the island. Until mid 2016, only three permanent seismic stations existed on the island. Pathak, Ravi Kumar, and Sarkar (2006) and Rai, Gaur, Rai, and Priestley (2009) analyzed receiver functions from the permanent station PALK and estimated Moho depth and Vp/Vs ratio. Prasanna, Chen, and z (2013) used gravity inversion and Mishra, Vijaya Kumar, and Rajasekhar (2006) modeled gravity anomalies within Sri Lanka and other continental fragments of Gondwana to determine the crustal thickness and structure beneath the island.

In 2016–2017 the Geological Survey and Mines Bureau (GSMB) of Sri Lanka and the German Research Centre for Geosciences (GFZ) installed and maintained the first broadband seismic network on the island (Fig. 1), consisting of 30 stations running for a period of 13 months. Here, we image the crustal structure of Sri Lanka using the new seismic data. We performed a joint inversion of dispersion curves from seismic ambient noise with receiver functions using a Bayesian approach, which allows us to compute a collection of possible models and to estimate the uncertainty of the model parameters.

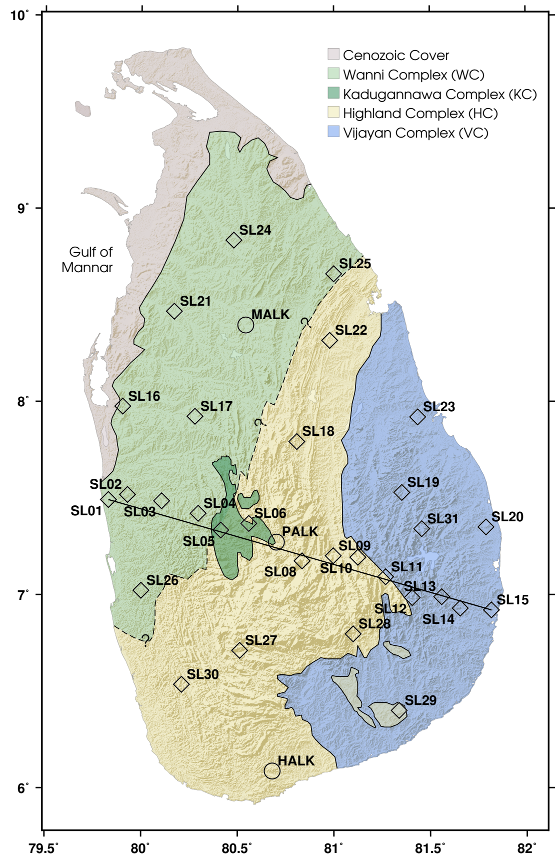

Figure 1. Map of seismic stations and major lithotectonic units (modified after Dissanayake & Chandrajith, 1999) in Sri Lanka. Diamonds represent station locations of temporary seismic array (FDSN code: 1A, 2016–2017). Circles denote three permanent stations (MALK, PALK, HALK). Black line indicates profile location for a cross section.

1.1 Geologic Background

Sri Lanka is mostly composed of Precambrian crust; only the northern and northwestern coasts show younger Jurassic-Quaternary sedimentary deposits (Fig. 1). The Precambrian basement consists of three major units, namely, from west to east, the Wanni Complex (WC), the Highland Complex (HC), and the Vijayan Complex (VC). Some HC erosion remnants (Klippen) occur around Buttala, Kataragama and Kuda Oya in the southern part of the VC. The Kadugannawa Complex (KC) is a relatively small unit located between the WC and HC. It is contentious whether it is part of the WC, part of the HC or the root zone of an island arc (**?**, and references therein). The WC/HC represents as a combined unit a tilted section of the former lower–middle crust, with the HC representing the lower level. The KC is at a crustal level between the WC and the HC (Kriegsman, 1994; Sandiford, Powell, Martin, & Perera, 1988; **?**). The WC consists of metamorphic rocks of upper amphibolite- to granulite-facies, the HC predominately of granulite facies and the VC of amphibolite facies (K. W. Kehelpannala, 2003, and references therein).

The contact between the WC and the HC is controversial due to absence of a structural break between them. Stretching lineations, shear sense indicators and sheath folds demonstrate that a collision has occurred in a NNW-SSE direction, i.e., the WC/KC was moving on top of the HC from NNW towards SSW (K. W. Kehelpannala, 2003, and references therein). The boundary between the WC and the KC is less clear, while that between the KC and the HC is well defined. The boundary between the HC and the VC is considered to be a deep crustal, sub-horizontal ductile shear / thrust zone (K. W. Kehelpannala, 2003; Kleinschrodt, 1994, 1996, and references therein). E-W stretching lineations in the VC and nearly N-S stretching lineations and shear sense indicators at and close to the shear zone suggest a nearly E-W directed transpressional collision between the combined WC/HC unit and the VC (**?**, and references therein). The general trend of subhorizontal fold envelopes suggests the thrust to underlie large parts of the HC; Klippen south of the HC prove that the thrust plane extended nearly up to the south coast (Kleinschrodt, 1994, 1996). Furthermore, Kleinschrodt (1994) suggests that the HC climbed on top of the east-VC with a ramp-flat geometry or a low-angle thrust, steepening to higher crustal levels.

The amalgamation of the Sri Lankan complexes took place within the framework of the Pan-African continental collision between West and East Gondwana. Petrological, geochemical and geochronological studies suggests that the WC, KC and VC have been formed through arc-related events during the Early Neoproterozoic, i.e., ∼1.0 Ga (Takamura, Tsunogae, Santosh, Malaviarachchi, & Tsutsumi, 2016, and references therein). A well-established theory for the amalgamation of Sri Lanka suggests a stepwise collision of the Precambrian arcs (e.g., K. V. W. Kehelpannala, 2004) during the Pan-African Orogeny, whereas Santosh et al. (2014) recently interpreted the WC, KC and VC as Early to Late Neoproterozoic continental arcs, with the HC as a Neoproterozoic suture zone formed by double-sided subduction and final collision of the WC and VC.

The hypothesis of the stepwise collision of the Precambrian arcs suggests an initial collision of the WC and HC fragments. As a unified block the WC/HC has experienced six phases of ductile deformation (D1–D6 in 0.61–0.55 Ga), which are not seen for the VC (**?**). The evidence therefore suggests an early stage collision of the WC/HC unit with the VC at D5 (0.58 Ga), and the WC/HC subsequently being thrust over the VC (K. W. Kehelpannala, 2003, and references therein). Based on post-tectonic intrusion by Cambrian granites and syenites through all three units, i.e., WC, HC and VC, the fragments of Sri Lanka were united at 0.55 Ga. Most of the older structures have been obliterated by strong Pan-African non-coaxial strain, which also brought all the early planar and linear fabrics into parallelism with those formed during the Pan-African event (**?**).

Based on petrological and geochemical data, Santosh et al. (2014) recently proposed an alternate scenario, termed divergent subduction, which involves a double-sided subduction of oceanic crust beneath the WC to the west and the VC to the east. The HC is therefore the collisional suture/ accretionary complex in between, where trench-fill sediments and ancient micro-continents or arcs are accreted and admixed during the final collision stage. Santosh et al. (2014) do not comment which larger lithospheric structures would be predicted by their model.

The Mannar Basin (west of Sri Lanka, partly onshore, Fig. 1) has been formed during Gondwana breakup, which initiated at approximately 165 Ma (**?**). A great amount of rifting between India and Sri Lanka together with strike slip movement and anticlockwise rotation of Sri Lanka was responsible for significant widening and rapid subsidence in the basin (Kularathna, Pitawala, Senaratne, Senevirathne, & Weerasinghe, 2015), and is associated with strong crustal thinning along the west coast.

1.2 Seismic Data

Until May 2016 the island of Sri Lanka was equipped with only three seismic stations: PALK, MALK and HALK. PALK is an IRIS/IDA station and operates since 2000 (**?**). MALK and HALK are GEOFON stations and have been operating since 2010 (**?**). In mid 2016 a field campaign was initiated by the GSMB of Sri Lanka and executed jointly with the GFZ (**?**). A network of 30 three-component broadband stations has been deployed (Fig. 1), which recorded continuous data for a period of 13 months.

The temporary array was designed to perform seismic ambient noise and receiver function analyses as well as local earthquake studies. Fourteen temporary stations and the permanent station PALK form a 230 km long profile across the island, from the west to the east coast, perpendicular to the predominant geologic strike (profile in Fig. 1). Interstation distances are about 15 km. Sixteen more stations were spread out on the island at a larger spacing of about 50 km.

Three stations (SL04, SL14, SL30) were operating only for a short period of time. SL14 failed after just 13 days, which was too short to record enough earthquake signals or to recover stable Green's functions; hence we excluded it from both analyses. Stations SL04 and SL30 were recording for 85 and 30 days, respectively. These stations were included for the ambient seismic noise analysis, but discarded for receiver function computation, as too few events occurred during operational time. The stations included in this study and the time period considered for further analyses are summarized in Table 1.

Table 1. Seismic broadband stations and time span included in this study. SR: sampling rate; SWD: Surface wave dispersion; RF: Receiver functions. The temporary network 1A is our primary data source.

Network	FDSN	Stations	SR (Hz)	SWD — Time Span — RF	
Temporary	1A	SL01−SL31	100	06/2016–06/2017	06/2016–06/2017
GEOFON	GE	MALK, HALK	50	05/2016–08/2017	01/2015–12/2017
IRIS/IDA	II	PALK	40	05/2016–08/2017	01/2015–12/2017

2 Seismic Ambient Noise Correlation and Tomography

In order to prepare the data for calculating the cross-correlation stacks, the linear trend and the mean were subtracted from the raw data and a low pass filter was applied prior to decimation to prevent aliasing effects. The threshold was set to 85 % of the new Nyquist frequency (2.125 Hz). The data were down-sampled to a sampling rate of 5 Hz, with subsequent instrument response removal.

For ambient noise cross-correlation we applied the pre-processing procedures suggested by Bensen et al. (2007). The instrument corrected data were clipped at 3 standard deviations and bandpass filtered between 0.01 and 1.25 Hz. Subsequently, spectral whitening and 1-bit normalization were applied. The cross-correlation was performed by correlating 1-hour segments of all station and component combinations and subsequently rotating the full Green's tensor stream from the ENZ to the RTZ coordinate system. The correlograms resulting from one day were added to daily stacks. Green's functions were generated by stacking the daily stacks for the time period available. This resulted in a final correlogram stack for each of the 496 station pairs and for each of the components. Here, we consider combinations of the radial and vertical component for the Rayleigh surface wave, i.e., vertical-vertical (ZZ), radial-radial (RR), vertical-radial (ZR), and radial-vertical (RZ).

Surface wave dispersion (SWD) was determined from the phase of the fundamental-mode Rayleigh wave, based on the zero-crossings of the real part of the correlation spectrum (Ekstrm, Abers, & Webb, 2009; **?**). The 2π ambiguity leads to a family of possible period–phase velocity relations. Therefore, the average phase velocity dispersion was computed for Sri Lanka and used as a guide for selection of the most likely branch for each station pair. To retrieve phase velocity measurements we used the tool GSpecDisp (Sadeghisorkhani, Gudmundsson, & Tryggvason, 2017). Dispersion curves were determined for the ZZ, RR, RZ, and ZR components, separately, resulting in 478, 422, 440, and 454 successful measurements, respectively. For 385 station pairs, all four components could be picked. To retrieve the final Rayleigh wave dispersion curve for each station pair, the four dispersion curves were averaged after interpolation.

The final 385 phase velocity dispersion curves for Sri Lanka are illustrated in Figure 2. The velocities increase from 2.9–3.3 km/s at the period of 1 s to 3.7–4.0 km/s at 30 s. The variations of phase velocities cover a narrow band with an average width of 0.35 km/s.

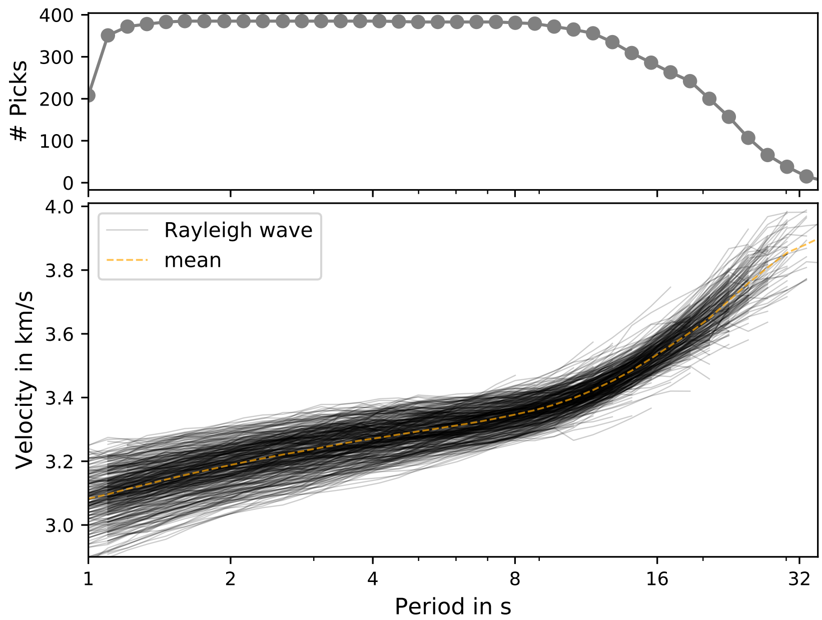

Figure 2. Rayleigh wave dispersion curves for all the individual station pairs (bottom). At most of the periods, the number of picks is >300 (top).

For travel time tomography we used the Fast Marching Surface wave Tomography package (FMST; Rawlinson & Sambridge, 2005; **?**). We gridded our study area into 12 x 15 cells, each having a dimension of ∼25 x 33 km. We considered five iterations, as the residuals rapidly decreased and stabilized. We assumed 2.5 % outliers, which were removed at the second iteration. As starting model each grid node was set to the period dependent mean velocity. (See SI for trade-off curves, Fig. S1, and outlier pre-selection.)

A selection of tomography results is illustrated in Figure S2. For shorter periods (1–8.5 s), velocity contours roughly follow the geological boundaries along a NNE-SSW direction. The highest velocities are around the WC/KC/HC contact and decrease with distance towards west and east. The lowest velocities are in the SE of the island. For periods longer than 10 s the pattern changes towards a north vs. south subdivision of velocity regions, instead of following the geologic boundaries.

Final dispersion curves were then constructed from the tomography results, corresponding to the locations of the seismic stations. These dispersion curves are smooth and stable up to a period of 30 s.

3 Receiver Functions and Hκ-Stack Analysis

We considered all earthquakes with magnitudes M>5.5 and epicentral distances of 30–90° (based on the USGS catalog). The temporary network recorded 246 of such earthquakes, the permanent stations registered 636 events. Most of the events are located NE-SE of Sri Lanka within a back azimuthal range of 40–120°, specifically along the West-Pacific and Indonesian plate boundaries. The data cover a slowness range of 4.6–8.8 s/°.

To ensure good quality receiver functions we selected seismograms with signal-to-noise ratio (SNR) >2.5. The selection process resulted in 1979 traces from 267 events (see Table S1). For receiver function (RF) computation, each trace was filtered (band pass: 0.05–5 Hz), decimated to a sampling rate of 20 Hz, and trimmed to 5 s before and 30 s after the P-onset. Subsequently, each trace was rotated from the ZNE into the LQT ray coordinate system based on the theoretical incidence angle assuming a surface Vs of 3.5 km/s. The Q-component was then deconvolved with the respective L component, utilizing water level stabilization (level: 0.001) and low pass filtering with a Gaussian function (Gauss factor: 1.0). The receiver functions were sorted according to slowness and stacked in bins of 0.2 s/° without amplitude normalization. The bin-stacked RFs show a coherent signal, as can be seen in Figure S3. The Q-RFs were not move out corrected for the final stack, as the move out correction has a strong effect on the multiple timing, which would result in biased interface depths in an inversion.

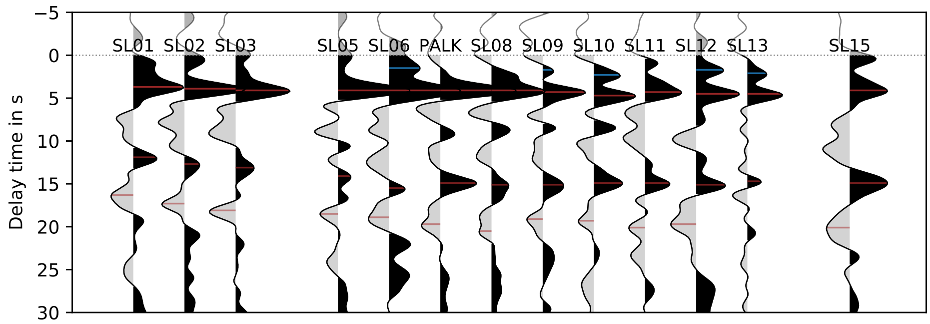

Figure 3. Receiver function stacks along main profile from SL01 to SL15. Brown markers indicate clear Ps converted phase at the Moho and corresponding multiples. Indications for a mid-crustal converter are marked in blue.

Receiver functions along the main profile are illustrated in Figure 3. The independently derived station stacks show consistent phases throughout the profile, especially regarding the Ps phase and its multiples. An intra-crustal phase (including first multiple) is visible at the central stations SL06–SL10 and fades at SL11–SL13. This intra-crustal arrival indicates a discontinuity with a strong velocity contrast at about 15–25 km depth.

The Hκ-stack grid search method following Zhu and Kanamori (2000) was applied to estimate Moho depths and Vp/Vs values. The method is illustrated in Figure S4 for a selection of stations. Moho depths for Sri Lanka range between 29.5–40 km with a typical uncertainty of ~2 km; for Vp/Vs the range is 1.6–1.82 with an average of 1.72 and a typical uncertainty of 0.06 (see Table S2). The Moho estimates strongly depend on the crustal Vp, which we assumed to be 6.5 km/s for each station; this is reasonable for felsic amphibolite and granulite facies continental crust (**?**). A misestimation of 0.1 km/s would result in a crustal thickness variation of about 1 km. The Vp/Vs ratios do not depend significantly on the assumed Vp.

4 Bayesian Inversion of SWD and RF

As a final step, receiver functions and phase velocity dispersion curves were jointly inverted with a Markov chain Monte Carlo (McMC) transdimensional Bayesian inversion tool (BayHunter; Dreiling & Tilmann, 2019), where we solve for the velocity-depth structure, the number of layers, the noise parameters, and the crustal average Vp/Vs. While other inversion methods often favor one best model based on the least misfit, an inversion after Bayes' theorem is based on the model's likelihood and results in probability distributions for each parameter of the model. The inversion result is represented by a collection of models, the posterior distributions of which form ideally Gaussian distributions if the chains have converged. For further details refer to **?** and to the documentation of BayHunter (Dreiling & Tilmann, 2019).

The model priors were set to a wide range, i.e., a depth range for the interfaces from the surface to 75 km, Vs from 2 to 5 km/s, and Vp/Vs from 1.45 to 2.05. Additionally, a maximum of 20 layers was imposed. The noise amplitude σ_{RF} spans from ~0 to 0.05, and σ_{SWD} from ~0 to 0.05 km/s. The correlation r for the correlated noise for RFs was fixed to a value of r_{RF}=0.96. For surface wave dispersion, the noise was assumed uncorrelated. The model priors turn out to be sufficiently wide, relative to the values with significant probability, i.e., none of the parameters inverted for have settled on a boundary.

The inversion was performed with 100 chains to ensure multiple independent parameter search paths. Each chain performed 1.8 million iterations, with a 2:1 ratio for the burn-in and exploration phase. The probability distributions for the proposal generation were adjusted during the inversion to maintain an acceptance rate of $\sim$40 %. Some chains failed to converge, returning significantly higher misfits than most chains after the burn-in phase. Such chains were declared as outlier chains. For the complete data set, $\sim$5 % of the chains were declared as outlier chains, which indicates that the chosen number of iterations was usually sufficient enough for the chains to converge properly. The final posterior distribution gathers 100,000 models from the main inversion phase by sub-sampling all non-outlier chains.

The posterior distribution of 100,000 models was sorted according to likelihood and categorized into three groups, including the best 25 %, 50 % and all models. Figure 4 shows an example of the McMC analysis for SL21, showing velocity-depth structures and corresponding data fits from randomly selected models from each group, and the posterior distributions of likelihood, joint misfit, SWD and RF noise amplitudes, number of layers and Vp/Vs for all models within a group. The grouping (colors) shows the compromises the algorithm made during an inversion, e.g., increasing the number of layers to reduce the noise level and the misfit. Each of the posterior parameters is unimodal. The surface wave dispersion shows a good data fit. For the receiver functions, the majority of modeled RF agrees very well in their signature, however, not all details of the waveform can be matched. The first order features are modeled in nearly every chain and the Vs-depth models show similar structures. The median model shows a sharp interface at 3 km depth and more gradual transitions at 13–15, 26–29 and 35–39 km; the gradual transitions imply a higher uncertainty about the correct interface depth. The Moho discontinuity lies between 35–39 km.

The quality of data fit for SL21 is representative for the other stations. (Data fits and average velocity-structures are shown for all stations in the SI, Figs. S5a, S5b and S6.) The posterior distributions are unimodal with the exception of the Vp/Vs of seven stations, which show bimodal distributions, and the Vp/Vs of one station (SL31), which did not yield plausible values (i.e., they settle on a boundary, even if extending the boundary to unrealistic values). Vp/Vs is a fine-tuning parameter, meaning, that the average Vs-depth structures we derived from our data set are relatively insensitive to Vp/Vs. For the seven stations showing bimodal Vp/Vs, the algorithm finds two Vp/Vs optima, and

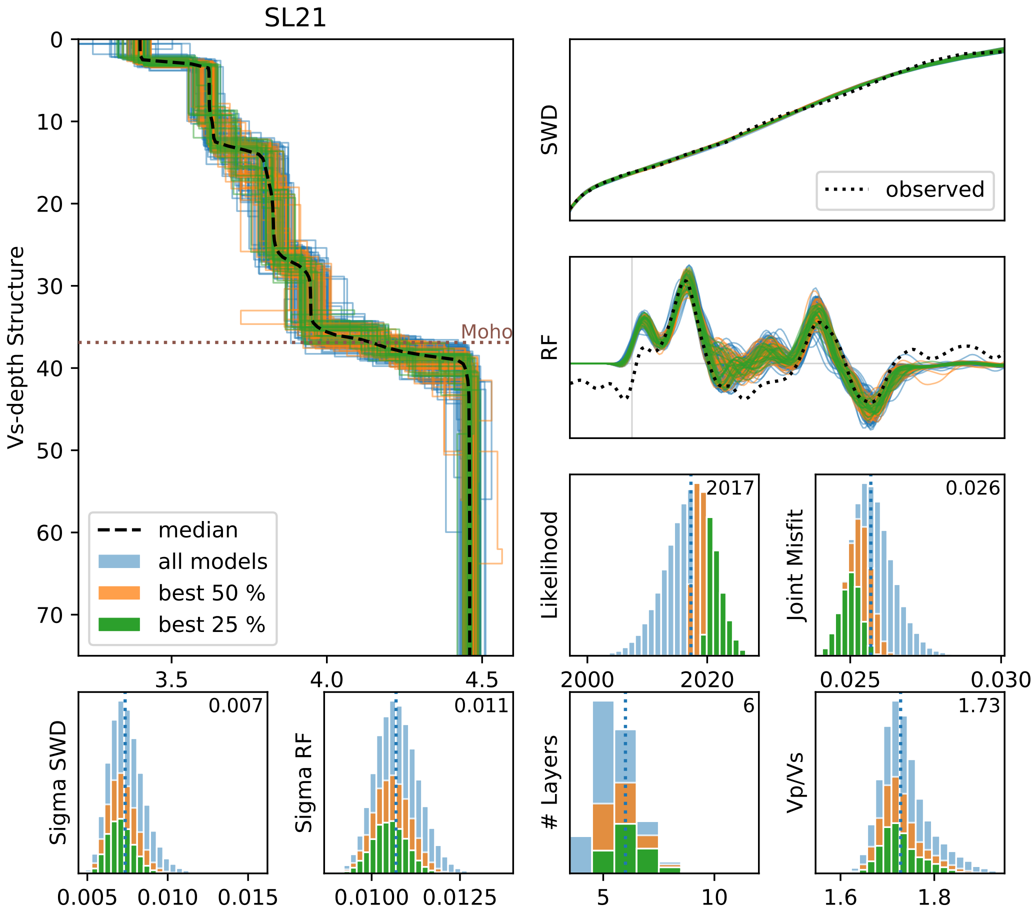

Figure 4. Selection of Vs models and corresponding data fits for station SL21, along with posterior distributions of likelihood, misfit, SWD and RF noise amplitudes, number of layers and Vp/Vs ratio. The results are color coded according to the likelihood, i.e., three groups showing 25 %, 50 % and 100 % of the best models. Dotted vertical lines illustrate the median, whose value is displayed in the upper right corner of each panel.

therefore compromises by slight modifications of the other parameters, but still leading to Gaussian distributions for Vs. The most probable Vs-depth models corresponding to either of the Vp/Vs optima, show equal major structures. For the station not converging in Vp/Vs, we compared the results with those from an inversion assuming a fixed Vp/Vs (=1.73), resulting in models that are very similar in their Vs-depth structure.

Figure 5a shows the posterior distribution for SL10 for the velocity-depth structures, including mean and mode model, and interface depth probabilities. The surface velocity is ∼3.4 km/s, the interfaces are well defined at 3, 12, 20, and 38 km. The Moho

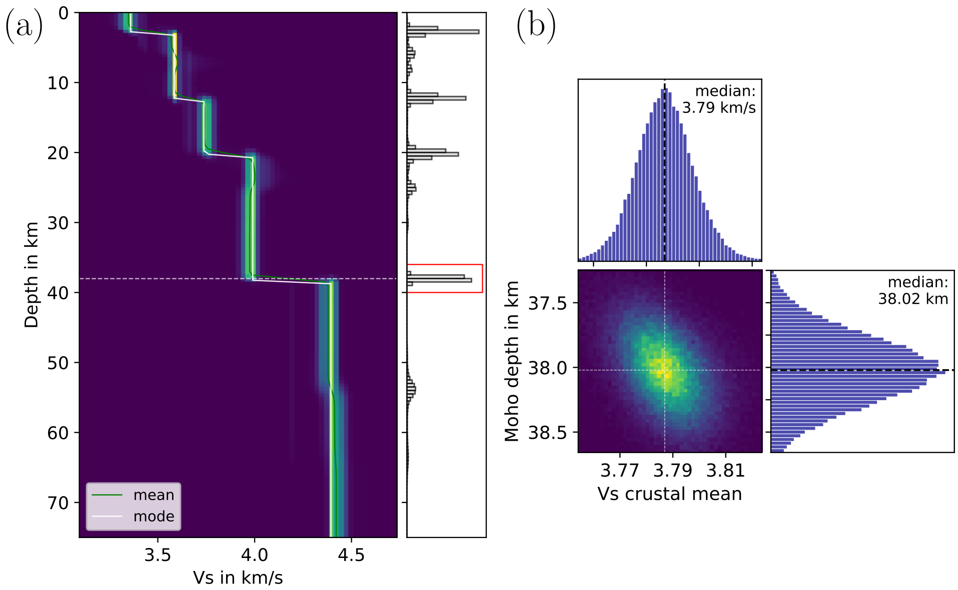

Figure 5. (a) Posterior distributions of shear wave velocities for station SL10 and interface depth probabilities. The red box marks the interface probability of the Moho. (b) Posterior distributions of the Moho depth and crustal average Vs. The median Moho depth is 38±0.2 km and the average crustal Vs is ∼3.79±0.01 km/s.

depth is between 37 and 39 km, emphasized by the red box in Figure 5a. To retrieve a robust estimate for the Moho depth, the Vs model of each station was inspected to give a pre-selected depth range (e.g., 37–39 km for SL10, 35–39 km for SL21). Each of the 100,000 models was then analyzed to find the interfaces within the pre-selected range, with the last crustal layer having a Vs <4.2 km/s. (See Fig. 5b for the distribution of Moho depths at SL10.) Additional parameters, e.g., Vs in the last crustal layer, average crustal Vs, Vs increase across the Moho and upper mantle Vs were extracted. Those values show a moderate trade-off between crustal thickness and velocity, as is illustrated in Figure 5b; although subtle, a deeper Moho estimate is accompanied by a larger average crustal Vs. This trade-off is well known for receiver functions, but reduced in its impact by the inclusion of surface wave dispersion. The Moho interface for SL10 is at 38±0.2 km and average crustal Vs is 3.79±0.01 km/s. Maps of median Moho depths and average crustal Vs are shown in Figure 6 with values as summarized in Table S2.

5 Crustal Velocity Structure

Figure 6 shows Moho depths and Vp/Vs derived by joint Bayesian inversions (a, b) and Hκ-stack analysis (d, e). Figure S7 illustrates a Vs cross section along the main profile (see Fig. 1 for profile location), comparing the differently derived Moho depths.

The Moho depths derived from joint inversion and Hκ-stacking generally agree well with each other. Absolute differences between both methods are between 0.1 and 3.2 km with a median difference of 0.7 km. The largest Moho depths (38–40 km) are found below the topographic high in the HC. The three northernmost stations in Sri Lanka (SL24, SL25, MALK) also have a deep Moho interface at $>\sim$38 km depth. The west coastal stations SL01–SL03 show the thinnest crust (30–35 km). SL20 at the east coast also shows a shallow Moho depth in the Hκ-stack ($\sim$33$\pm$2 km), but not in the joint inversion ($\sim$36 km). We note that there is a strong interface at $\sim$31 km depth that might have been interpreted as the Moho in the Hκ-stacking (Fig. 7b, right); this station has the largest Moho deviation of 3.2 km.

The Moho interface generally mirrors the topography, i.e., higher crustal elevations correspond to larger Moho depths (Fig. S7). The crustal thickness is continuously increasing from SL01 to SL05 (30–36 km), with a sudden increase of 3 km to 39 km at SL06, which corresponds to the topographic trend with an elevation change by a factor of 4 from SL05 to SL06. SL08 shows the deepest Moho interface, which is thus getting slightly shallower again towards the east coast.

The median Vp/Vs values from joint inversion are between 1.5–1.93, with the majority between 1.68–1.8. The Hκ-stack results range between 1.6–1.82, with the majority of the stations between 1.66–1.73. The differences of Vp/Vs from both techniques are up to 0.28 with a median difference of 0.03 km. Vp/Vs results from both methods agree in their general range for the study region, but do not show a common pattern. Hκ-stack results for Vp/Vs are more reliable, as they include a range of RFs and consider the arrival times of Ps conversion and multiples directly associated with the slowness. For joint inversion, we considered the RF stack with its median slowness.

The average crustal Vs (Fig. 6c) ranges from 3.7–3.9 km/s, with increased velocities in the central HC (>3.83 km/s), decreasing with distance towards the coastal regions. The southern and westernmost coastal stations (SL01, SL02, HALK) have the lowest crustal Vs. Moho depths, crustal average Vs and Vp/Vs do not show a clear correlation, neither with each other, nor with the surface geologic units.

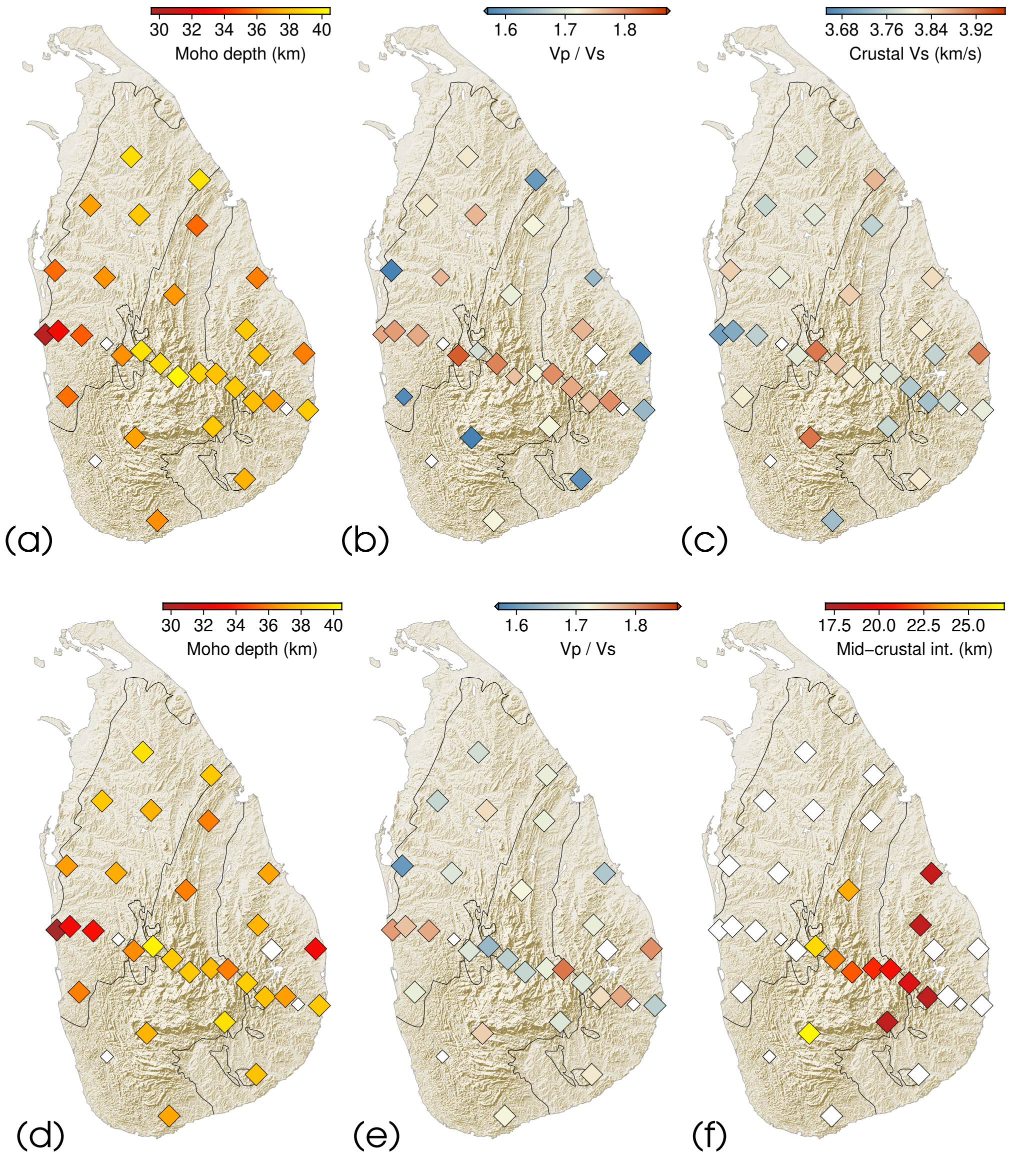

Figure 6. Spatial distribution of (a) Moho depths, (b) Vp/Vs ratio, (c) crustal average Vs and (f) mid-crustal interface depths derived from the McMC Bayesian inversion. (d) and (e) are the Moho depths and Vp/Vs ratios derived from the Hκ-stack grid search, respectively. White symbols denote stations with no inversion performed (small diamonds) or no results gained (large diamonds). The smaller colored symbols in (b) indicate that the distributions are bimodal.

The cross section in Figure 7a (and Fig. S7) shows a prominent westward dipping mid-crustal interface with an apparent angle of ∼4.3° between SL06–SL12, and an average velocity increase from 3.75 to 4 km/s. These lower crustal high velocities are absent at the stations adjacent to the west (SL01–SL05), while the stations to the east (SL11–SL13) show a thinner or inter-layered section of the higher velocities. The probability of interfaces (Fig. S7) furthermore suggest the dipping interface to be traceable across the entire profile (SL03–SL15). Figure 7a shows our interpretation of the intra-crustal interface; it is also evident on five other stations across Sri Lanka (Fig. 7b, left). Figure 6f shows the spatial extent of the mid-crustal discontinuity; values are summarized in Table S2.

The mid-crustal interface is observable on the central stations in the HC, and on three additional stations in the VC. For the stations in the HC the interface depth lies between ∼18–27 km; the interface in the VC is at ∼18 km depth. The strike has an orientation similar to the geologic strike with a dip towards WNW.

A well constrained low velocity zone is observed along SL05–SL09, and SL13 at depths of 10 km, with Vs between 3.4–3.6 km/s. Stations SL15, SL20, SL23, SL25 and SL26 show low velocity zones at mid- to lower crustal depths (20/30 km); they are located at the western and eastern coastlines.

6 Interpretation and Discussion

6.1 Comparison with other geophysical studies

The Hκ-stack analysis from Pathak et al. (2006) reveals a Moho depth of 34±1 km beneath PALK, much shallower compared to our results from two independent analyses, which are 38.25±1.9 km and 39±0.3 km from Hκ-stack and Bayesian inversion, respectively. This discrepancy can (partially) be explained by the average Vp they assumed for the crust (6.0 or 6.1 km/s?), which is lower than our Vp assumption of 6.5 km/s. Rai et al. (2009) obtained a crustal thickness of 37.5±1 km and Vp/Vs value of 1.721±0.02 for PALK. Their estimates of Moho depth and Vp/Vs agree borderline with ours. By forward and inverse modeling of RF and surface wave data they inferred a velocity-depth structure with a low velocity layer in the upper crust and a mid-crustal discontinuity at a depth of 22.5 km. We also observe a shallow low velocity zone (∼10 km) and an intra-crustal discontinuity at 23±0.4 km.

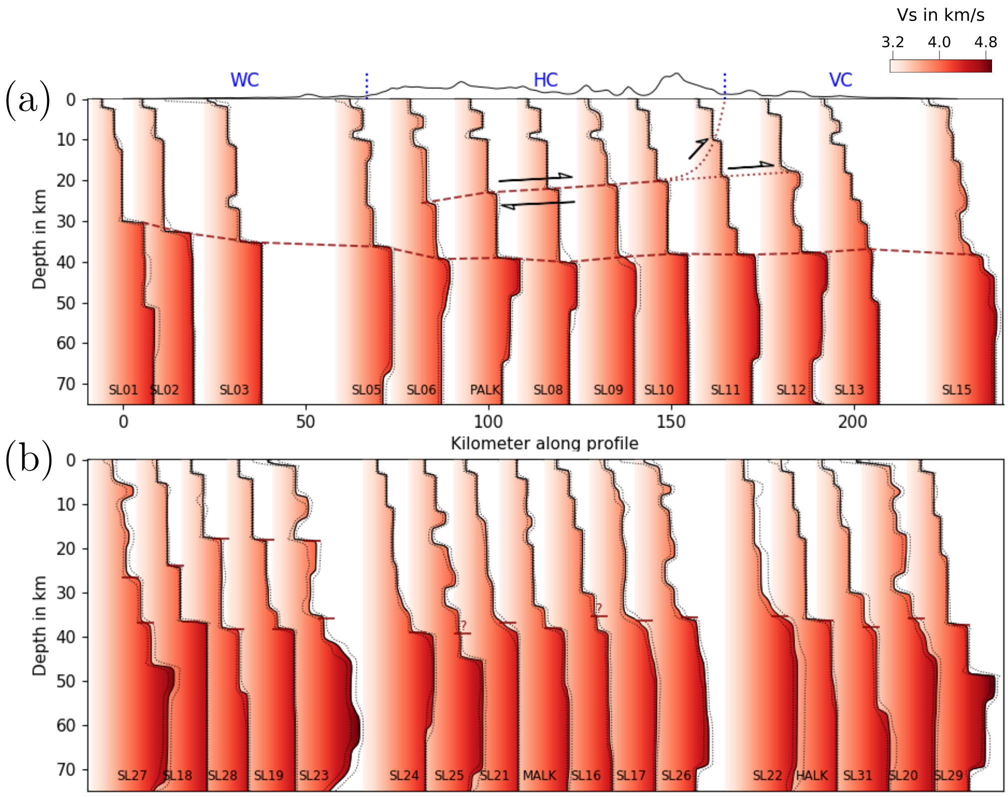

Figure 7. Vs models at stations along the main profile (a) and at other stations away from the profile (b). The shallow and deeper red markers indicate the mid-crustal and Moho interface, respectively. The dotted lines mark an interpretation of the outcropping mid-crustal interface, and a possible continuation within the crust. Shear sense indicators denote an ancient thrust. The Vs models in (b) are divided into 3 groups, from left to right, with stations that include the mid-crustal interface, stations in the WC, and stations located in the HC and VC, respectively. Moho depths labeled with a question mark indicate an interpretation leaned on surrounding stations (see also SL13).

Mishra et al. (2006) used gravity data and modeled the anomalies along an E-W profile through PALK. They modeled crustal thicknesses of up to 40–41 km under the eastern part of the HC, close to our observations, and explain the central gravity high with a higher density crustal section protruding in the upper crust (10–15 km). We also observe a central anomalous higher velocity section (which can correlate to higher densities), however, situated in the lowermost crust. A fresh gravity modeling based on our results might be of interest, but would exceed the scope of this study.

6.2 Average crustal Vp/Vs

Vp/Vs can be helpful to distinguish between felsic and mafic rocks as a matter of the relative proportions of quartz (Vp/Vs∼1.49) and plagioclase (Vp/Vs∼1.87) (Christensen, 1996). Musacchio, Mooney, Luetgert, and Christensen (1997) grouped crustal rocks based on Vp/Vs and Vp into three categories: felsic, anorthositic and mafic rocks.

Classifying the results from Hκ-stacking, none of the Vp/Vs lies beyond 1.82, which would exclude an anorthosite rock composition. As our Vp/Vs for both analyses are generally more on the lower end (1.66–1.73 and 1.68–1.8), most of Sri Lanka is represented by felsic rocks with intermediate-to-high silica content. However, our Vp/Vs estimates are crustal averages; it is possible that sections of the crust are dominated by different compositions. The joint inversion shows average crustal Vs between 3.7–3.9 km/s (Vp: 5.9–7.3 km/s), which would predominantly still favor a felsic composition over a mafic one.

6.3 Moho depths and intra-crustal features

The Moho depths are not obviously correlated with the geologic units, which suggests that the crustal fragments have been unified through reworking and deformation through the Pan-African collision and possibly later erosive processes. The Moho interface generally mirrors the topography, except for the thicker crust in the northernmost part of the island, which might be caused by density differences through crustal composition. The thinner crust along the west coast (<36 km), including the thinnest crust at SL01–SL03 (30–35 km), can be explained by the formation of the adjacent Mannar Basin, including rifting and crustal thinning.

Our study reveals a major WNW-dipping mid-crustal interface in the central HC with an apparent dip of ∼4.3° along the profile. Stations in the VC and close to the HC/VC border (i.e., SL12, SL19, SL23, SL28) also show a discontinuity at a depth of ∼18 km. It is unclear whether the four stations see the same structure as the stations in the HC or image a separate feature within the eastern VC. The mid-crustal interface might be a feature from before the Pan-African collision; however, as the extent of the discontinuity from the HC into the eastern VC continues at the same depth and shows coherent Vs contrast, it is likely that the interface is the result of a shared event. Therefore, we are inclined to interpret this mid-crustal feature as being related to the HC/VC thrust contact.

Kleinschrodt (1994, 1996) suggested that the HC was thrust onto the eastern VC along a deep crustal, sub-horizontal to gently west-dipping thrust surface, which underlies large parts of the HC, with a thrust geometry of a ramp-flat geometry or a low-angle thrust that steepens to higher crustal levels. Our results are in agreement with this hypothesis, which is supported by several other studies (see introduction). The interface might be interpreted as the HC/VC thrust contact that steepens to shallower crustal levels and the surface (Fig. 7a). Stations SL11-SL13 show a slightly different Vs structure below the discontinuity (Fig. S7), i.e., high Vs inter-layered with lower Vs, which could reflect the complicated contact zone between the HC and VC and might even image a buried continuation of the thrust contact within the VC, i.e., a blind thrust.

A low velocity layer as we observe at the central stations within the HC, was also observed by Rai et al. (2009) in the upper crust of other Pan-African terranes. Such intra-crustal structure is assumed to be a relic of deformation and magmatism caused by upwelling of lower crust or subcrustal melts. Low velocity zones are thought to be the consequence of an influx of CO_2-rich fluids, that are trapped at these depths or originated from retrograde metamorphism to amphibolite and greenschist facies, and were brought there through deep-seated thrusting and lateral shearing during a transpressive regime (Rai et al., 2009, and references therein).

6.4 The amalgamation of Sri Lanka

The hypothesis of the stepwise collision predicts westwards dipping thrust contacts between the WC/KC, the HC and the VC island arcs (e.g., K. V. W. Kehelpannala, 2004). We observe a gently westward dipping mid-crustal interface beneath the HC which shows a strong Vs increase and thus indicates a change of rock material. Our observation matches the proposed position and orientation of the HC/VC thrust contact. The velocity change is also seen within the eastern VC, which suggests that the structure might has been part of the VC crust before thrusting, or evolved alongside. We assume a steepening of the thrust contact to the surface; as the signature of the mid-crustal interface in the central HC does not disappear, but fades towards the east, we propose a buried continuation within the VC. The low velocity layer in the HC along the main profile ($\sim$10 km depth) might be caused by influx of CO_2-rich fluids of retrograde metamorphism to amphibolite facies brought about by deep-seated thrusting and lateral shearing during a transpressive regime. The dipping mid-crustal interface and the low velocity zone, both relate to deeper thrusting and a transpressive regime, which clearly favors the stepwise collision theory as described with its details (see section 1.1).

Does this exclude the possibility of an amalgamation through divergent double subduction? Santosh et al. (2014) sketch the amalgamation with processes such as slab melting and arc magmatism, basaltic underplating, astenospheric upwelling and slab break-off; features, that are also included in the stepwise collision and we cannot asses with our data. In their study, Santosh et al. (2014) did not focus on crustal structures, which makes it impossible for us to discuss the matter based on their information.

Divergent double subduction occurs rather rarely (e.g., the Lachlan fold belt in southern Australia, the Molucca Sea collision zone in Indonesia). Also, a large scale dipping structure in the accretionary zone is not a feature seen for this type of subduction (e.g., **??**); however, the crustal structure is mostly not the focus of these studies. As argued above, we prefer the stepwise collision hypothesis, although we cannot completely exclude the theory of the double-sided subduction.

7 Conclusions

Rayleigh wave dispersion curves from ambient noise correlation and receiver functions were computed and jointly inverted using McMC transdimensional Bayesian inversion. Based on the median of the posterior distributions received from each station, we evaluated the crustal velocity structure of Sri Lanka.

Our results show a Moho interface at 30–40 km depth with a distinct velocity increase. The Moho depths show no correlation to the geologic units and largely mirror the topography, which suggests Airy isostacy for most of the Sri Lankan continental crust. A thicker crust in the northernmost part of the island might be caused by compositional effects on density. The lower Moho depths along the west coast emerged presumably through rifting and crustal thinning processes through the formation of the adjacent Mannar Basin.

We identify a prominent intra-crustal interface beneath the HC (18–27 km), and the eastern VC (∼18 km). We relate this westward dipping interface to the HC/VC thrust contact, which steepens to shallower crustal levels. The interface within the VC might have been part of the VC unit before the thrusting event, or evolved alongside. A low velocity zone in the central HC supports deep-seated thrusting and lateral shearing during a transpressive regime. Our results clearly favor the amalgamation theory of a stepwise collision of arc fragments to form Sri Lanka.

Acknowledgments

Many thanks to Dr. Robert Trumbull for the vivid discussions about geologic interrelationships. We thank the GSMB of Sri Lanka, which made it possible to deploy a temporary seismic network in Sri Lanka, and the employees for their local support and engagement during the field work. We acknowledge the GFZ for funding the field experiment from expedition funds, the Geophysical Instrument Pool Potsdam (GIPP) for supplying the instruments, the GEOFON data center for hosting the project data (`https://geofon.gfz-potsdam.de/waveform/archive`), and DFG research support through grant TI316/4-1.

References

Bensen, G. D., Ritzwoller, M. H., Barmin, M. P., Levshin, A. L., Lin, F., Moschetti, M. P., ... Yang, Y. (2007, June). Processing seismic ambient noise data to obtain reliable broad-band surface wave dispersion measurements. *Geophysical Journal International*, *169*(3), 1239–1260. Retrieved 2016-05-12, from `http://gji.oxfordjournals.org/cgi/doi/10.1111/j.1365-246X.2007.03374.x` doi: 10.1111/j.1365-246X.2007.03374.x

Christensen, N. I. (1996). Poisson's ratio and crustal seismology. *Journal of Geophysical Research: Solid Earth*, *101*(B2), 3139–3156. Retrieved 2019-02-06, from `https://agupubs.onlinelibrary.wiley.com/doi/abs/10.1029/95JB03446` doi: 10.1029/95JB03446

Curray, J. R. (1984). Sri Lanka: is it a Mid - Plate Platelet? Retrieved 2019-01-24, from `https://core.ac.uk/download/pdf/33720749.pdf`

Dissanayake, C. B., & Chandrajith, R. (1999, March). Sri LankaMadagascar Gondwana Linkage: Evidence for a PanAfrican Mineral Belt. *The Journal of Geology*, *107*(2), 223–235. Retrieved 2017-11-24, from `http://www.journals.uchicago.edu/doi/10.1086/314342` doi: 10.1086/314342

Dreiling, J., & Tilmann, F. (2019). *BayHunter - McMC transdimensional Bayesian inversion of receiver functions and surface wave dispersion.* GFZ Data Services. Retrieved 2019-05-27, from `http://dataservices.gfz-potsdam.de/panmetaworks/showshort.php?id=escidoc:3928900` doi: 10.5880/

GFZ.2.4.2019.001

Eaton, D., Milkereit, B., & Salisbury, M. (2003). *Hardrock Seismic Exploration.* Society of Exploration Geophysicists. Retrieved from https://books.google.de/books?id=cGeN03ZbmPYC

Ekstrm, G., Abers, G. A., & Webb, S. C. (2009, September). Determination of surface-wave phase velocities across USArray from noise and Aki's spectral formulation. *Geophysical Research Letters*, *36*(18), L18301. Retrieved 2017-05-15, from http://onlinelibrary.wiley.com/doi/10.1029/2009GL039131/abstract doi: 10.1029/2009GL039131

Haberland, C., Seneviratne, M., & Dreiling, J. (2016). *Sri Lanka temporary broad-band network.* GFZ Data Services. Retrieved 2019-05-24, from http://geofon.gfz-potsdam.de/doi/network/1A/2016 doi: 10.14470/6N7561723039

He, X.-F., Santosh, M., Tsunogae, T., Malaviarachchi, S. P., & Dharmapriya, P. (2016, July). Neoproterozoic arc accretion along the eastern suture in Sri Lanka during Gondwana assembly. *Precambrian Research*, *279*, 57–80. Retrieved 2019-05-13, from https://linkinghub.elsevier.com/retrieve/pii/S0301926816300547 doi: 10.1016/j.precamres.2016.04.006

Herath, P., Gunatilake, J., & Weerasinghe, D. (2017). Mohorivicic discontinuity beneath Mannar Basin: A failed-rift. , *18*, 12.

Kehelpannala, K. V. W. (2004). Arc Accretion Around Sri Lanka During the Assembly of Gondwana. *Gondwana Research*, *7*(4), 7.

Kehelpannala, K. W. (2003). Structural evolution of the middle to lower crust in Sri Lanka-a review. *ResearchGate*, *11*. Retrieved 2019-02-06, from https://www.researchgate.net/publication/284313338_Structural_evolution_of_the_middle_to_lower_crust_in_Sri_Lanka-a_review

Kleinschrodt, R. (1994). Large-scale thrusting in the lower crustal basement of Sri Lanka. *Precambrian Research*, *66*(1-4), 39–57.

Kleinschrodt, R. (1996). Strain localization and large-scale block rotation in the lower continental crust, Kataragama area, Sri Lanka. *Terra Nova*, *8*(3), 236–244. Retrieved 2019-05-13, from https://onlinelibrary.wiley.com/doi/abs/10.1111/j.1365-3121.1996.tb00752.x doi: 10.1111/j.1365-3121.1996.tb00752.x

Kriegsman, L. M. (1994, February). Evidence for a fold nappe in the high-grade basement of central Sri Lanka: terrane assembly in the pan-african lower crust? *Precambrian Research*, *66*(1-4), 59–76. Retrieved 2019-05-24, from https://linkinghub.elsevier.com/retrieve/pii/0301926894900442 doi: 10.1016/0301-9268(94)90044-2

Kularathna, E., Pitawala, H., Senaratne, A., Senevirathne, B., & Weerasinghe, D. (2015). Forced-fold structures in the Mannar Basin, Sri Lanka: Modes of occurrence, development mechanism and contribution for the petroleum system. , *17*, 12.

Mishra, D., Vijaya Kumar, V., & Rajasekhar, R. (2006, August). Analysis of airborne magnetic and gravity anomalies of peninsular shield, India integrated with seismic and magnetotelluric results and gravity anomalies of Madagascar, Sri Lanka and East Antarctica. *Gondwana Research*, *10*(1-2), 6–17. Retrieved 2019-02-06, from https://linkinghub.elsevier.com/retrieve/pii/S1342937X06000979 doi: 10.1016/j.gr.2005.11.014

Musacchio, G., Mooney, W. D., Luetgert, J. H., & Christensen, N. I. (1997). Composition of the crust in the Grenville and Appalachian Provinces of North America inferred from Vp/Vs ratios. , *102*. Retrieved 2019-05-22, from https://escweb.wr.usgs.gov/share/mooney/1997_Composition%20Crust%20Grenville-Appalachian.pdf

Nick Rawlinson. (2005). *FMST: Fast Marching Surface Tomography Package - Instructions.* Research School of Earth Sciences, Australian National University, Canberra ACT 0200. Retrieved from http://rses.anu.edu.au/~nick/surftomo/instructions.pdf

Pathak, A., Ravi Kumar, M., & Sarkar, D. (2006, August). Seismic structure of Sri Lanka using receiver function analysis: A comparison with other high-grade Gondwana terrains. *Gondwana Research*, *10*(1), 198–202. Retrieved 2017-11-24, from http://www.sciencedirect.com/science/article/pii/S1342937X06001134 doi: 10.1016/j.gr.2005.10.006

Prasanna, H. M. I., Chen, W., & z, H. B. (2013, September). High resolution local Moho determination using gravity inversion: A case study in Sri Lanka. *Journal of Asian Earth Sciences*, *74*(Supplement C), 62–70. Retrieved 2017-12-12, from http://www.sciencedirect.com/science/article/pii/S1367912013003192 doi: 10.1016/j.jseaes.2013.06.005

Premarathne, U., Suzuki, N., Ratnayake, N., & Kularathne, C. (2016, April). BURIAL AND THERMAL HISTORY MODELLING OF THE MANNAR BASIN, OFFSHORE SRI LANKA. *Journal of Petroleum Geology*, *39*(2), 193–213. Retrieved 2019-05-21, from `http://doi.wiley.com/10.1111/jpg.12640` doi: 10.1111/jpg.12640

Rai, A., Gaur, V. K., Rai, S. S., & Priestley, K. (2009, February). Seismic signatures of the Pan-African orogeny: implications for southern Indian high-grade terranes. *Geophysical Journal International*, *176*(2), 518–528. Retrieved 2018-09-03, from `https://academic.oup.com/gji/article-lookup/doi/10.1111/j.1365-246X.2008.03965.x` doi: 10.1111/j.1365-246X.2008.03965.x

Rawlinson, N., & Sambridge, M. (2005). The fast marching method: an effective tool for tomographic imaging and tracking multiple phases in complex layered media. *Exploration Geophysics*, *36*(4), 341. Retrieved 2016-11-08, from `http://www.publish.csiro.au/?paper=EG05341` doi: 10.1071/EG05341

Sadeghisorkhani, H., Gudmundsson, O., & Tryggvason, A. (2017, September). GSpecDisp: A matlab GUI package for phase-velocity dispersion measurements from ambient-noise correlations. *Computers & Geosciences*. Retrieved 2017-10-04, from `http://www.sciencedirect.com/science/article/pii/S009830041730119X` doi: 10.1016/j.cageo.2017.09.006

Sandiford, M., Powell, R., Martin, S. F., & Perera, L. R. K. (1988). Thermal and baric evolution of garnet granulites from Sri Lanka. *Journal of Metamorphic Geology*, *6*(3), 351–364. Retrieved 2019-05-13, from `https://onlinelibrary.wiley.com/doi/abs/10.1111/j.1525-1314.1988.tb00425.x` doi: 10.1111/j.1525-1314.1988.tb00425.x

Santosh, M., Tsunogae, T., Malaviarachchi, S. P., Zhang, Z., Ding, H., Tang, L., & Dharmapriya, P. (2014, December). Neoproterozoic crustal evolution in Sri Lanka: Insights from petrologic, geochemical and zircon UPb and LuHf isotopic data and implications for Gondwana assembly. *Precambrian Research*, *255*, 1–29. Retrieved 2018-08-31, from `http://linkinghub.elsevier.com/retrieve/pii/S0301926814003337` doi: 10.1016/j.precamres.2014.09.017

Takamura, Y., Tsunogae, T., Santosh, M., Malaviarachchi, S. P. K., & Tsutsumi, Y. (2016, August). UPb geochronology of detrital zircon in metasediments from Sri Lanka: Implications for the regional correlation of Gondwana fragments. *Precambrian Research*, *281*, 434–452. Retrieved 2019-02-15, from http://www.sciencedirect.com/science/article/pii/S0301926816302030 doi: 10.1016/j.precamres.2016.06.015

Wilbert Kehelpannala, K. V. (1997, October). Deformation of a High-Grade Gondwana Fragment, Sri Lanka. *Gondwana Research*, *1*(1), 47–68. Retrieved 2019-05-09, from http://www.sciencedirect.com/science/article/pii/S1342937X05700058 doi: 10.1016/S1342-937X(05)70005-8

Zhu, L., & Kanamori, H. (2000). Moho depth variation in southern California from teleseismic receiver functions. *Journal of Geophysical Research*.